Attachment 4

RELEASED FOR USNRC REVIEW 2018/01/26

CDM Apvd

30441R00021
Revision C

REACTOR-BASED MOLYBDENUM-99 SUPPLY SYSTEM PROJECT

TARGET ASSEMBLY THERMAL ANALYSIS

Prepared by General Atomics
for the U.S. Department of Energy/National Nuclear Security Administration and Nordion Canada Inc.

Cooperative Agreement DE-NA0002773

[redacted]

GA Project 30441
WBS 1110

GENERAL ATOMICS

MURR® Matters...

nordion

REVISION HISTORY

Revision	Date	Description of Changes
A	24OCT16	Initial Release
B	25JAN17	Revised to Address MURR Comments
C	26JAN18	Revised to address changes in target pellet manufacturing tolerances

POINT OF CONTACT INFORMATION

PREPARED BY:			
Name	**Position**	**Email**	**Phone**
Howard Chiger	Engineer	Howard.Chiger@ga.com	858-455-3231
APPROVED BY:			
Name	**Position**	**Email**	**Phone**
B. Schleicher	Chief Engineer	Bob.Schleicher@ga.com	858-455-4733
K. Murray	Project Manager	Katherine.Murray@ga.com	858-455-3272
K. Partain	Quality Engineer	Katherine.Partain@ga.com	858-455-3225

DESIGN CONTROL SYSTEM DESCRIPTION

		DISC	QA LEVEL	SYS
☐	R & D			
☒	DV&S			
☐	DESIGN			
☐	T&E	N	II	N/A
☐	NA			

TABLE OF CONTENTS

LIST OF FIGURES

LIST OF TABLES

ACRONYMS

Acronym	Description
ASME B&PV	Boiler and Pressure Vessel Code of the American Society of Mechanical Engineers
CHF	Critical Heat Flux
CHFR	Critical Heat Flux Ratio
CL	Center Line
CTE	Coefficient of Thermal Expansion
D_h	Hydraulic Diameter
G	Thermal conductance between two points
HTC	Heat Transfer Coefficient
k	Thermal Conductivity
$k_{effective}$	Combined conduction and convection, expressed as a conductivity
LOFC (LOPF)	Loss of Forced Cooling (same as/due to Loss of Pump Flow)
MH	Maximum Heating (one of two "worst case" rod analysis cases)
NIST	National Institute of Standards and Technology
PLP	Peak Linear Power (one of two "worst case" rod analysis cases)
Q_{norm}	Normalized local heat generation rate
Re (D_h)	Reynolds number based on hydraulic diameter
T	Temperature
TD	Theoretical (100%) Density
Q	Heat
ΔT	Temperature difference between two points

[redacted]

1 OBJECTIVE

The Target Assembly consists of an aluminum and steel cartridge containing 11 overlapping holes, each of which contains a Zircaloy-4 tube filled with heat generating UO_2 pellets, as shown in Figure 1. Helium gas inside the tubes fills the gaps between the Zircaloy and UO_2. The entire system is cooled by water flowing axially along the outside of the tubes in the scalloped holes.

Figure 1. The target cartridge filled with rods

Neutronics analyses (30441R00031) have been performed to determine the total power produced in the cartridge rods. Since the target power and linear heat flux can vary depending on changes in the reactor fuel burnup, control rod position and beryllium age, the maximum target fission power and maximum linear heat rate for the reactor operating at 10 MWt (as defined in 30441R00031) was used as the basis for the thermal hydraulic design.

The maximum total power dissipated in the cartridge was used to set the water flow rate in the cartridge such that there would be approximately a 10°C (18°F) temperature difference between its inlet and exit temperatures at 10 MWt reactor power and nominal reactor conditions. This flow rate shall be maintained, ±5%, at all times, with a ±15% allowable range being the set points for a reactor scram. Cartridge inlet water shall be taken from the reactor pool and cooled in a heat exchanger by ~10°C, so as to exit the cartridge at the pool temperature, and thus have little or no effect on the overall heat balance of the reactor cooling system. There are two cartridge locations in the reactor, and they may have between 3 and 11 UO_2 filled rods in them (with each cartridge having the same number of rods). If there are less than 11 UO_2 filled rods in the cartridge, "blank", non-fissioning, non-heat generating rods shall be inserted in the place of the missing rods to maintain the hydraulic integrity of the system.

The objective of this analysis is to determine the thermal hydraulic characteristics of the assembly and the temperatures in the uranium pellets, Zircaloy cladding and cooling water for a variety steady state operating scenarios:

- At nominal (10 MWt) and maximum (11.5 MWt) reactor power
- At nominal (100%) and minimum (85%) rate water flow
- At the nominal, minimum and maximum gaps between the Zircaloy and UO_2 that dimensional stack ups dictate
- With minimum, nominal and maximum scalloped water channel diameters that dimensional stack ups dictate

- With the minimum and maximum number of operating rods in the cartridge

- For the rods with the highest local linear peak power in the cartridge and with the highest total power in the cartridge

- For the expected and worst cases (with maximum error margins)

For all analyses, the maximum allowable UO_2 temperature is 2400°C and the Critical Heat Flux Ratio (CHFR) of the local Critical Heat Flux (CHF) to the actual local heat flux shall be at least 2.0.

Note that the term "nominal" is used here to describe expected operating and geometric conditions. For example, the nominal reactor power is 10 MWt. The nominal coolant flow rate is 100%. The nominal geometry is the dimension without allowable manufacturing tolerances. Analyses were run at both nominal and off-nominal conditions for the rods with both the peak linear and maximum total power. Note, too, that all the dimensions referenced are of the room temperature assembly, but that these dimensions change as the unit heats up, and the actual analyses were performed at operating dimensions.

2 APPLICABLE DOCUMENTS

A list of applicable documents is provided below.

Document Number	Document Title
30441D00207	Target System Cladding
30441D00211	Target System Pellet
30441R00017	ANSYS Target Cartridge, Housing Structural Analysis Design Calculation Report
30441R00022	Source Term Analysis Design Calculation Report
30441R00029	SINDA 85 (V2.2) Software Verification Test Report
30441R00031	Mo-99 Target Assembly Nuclear Design for Once-Through Operation
30441R00038	Computational Fluid Dynamics Analysis Of Target Housing Design Calculation Report

3 ASSUMPTIONS AND ANALYSIS DESIGN BASIS

Table 1 lists the heating rates for the rod in the cartridge with the peak local linear power, the rod with the highest total power, and the "average" rod at 10 MWt reactor power, derived from 30441R00031. These values have been maximized to include allowances for statistical variations in the pellets and analysis.

[redacted]

Table 1
Summary of 10 MWt Pellet Heating Values

	Peak Linear Power Rod	Max Power Rod	Average Rod	
Peak pellet linear power, kW/m	[redacted]	[redacted]	[redacted]	
Average pellet linear power, kW/m	[redacted]	[redacted]	[redacted]	5a, d, e, f
Average pellet power density, W/cc	[redacted]	[redacted]	[redacted]	
Rod total heat, W	[redacted]	[redacted]	[redacted]	
Peak power density, W/cc	[redacted]	[redacted]	[redacted]	
Fraction of heat below hottest location	0.354	0.479	0.453	
Fraction of rod length below hottest location	0.300	0.460	0.420	
Max heat flux at cladding OD, MW/m^2	[redacted]	[redacted]	[redacted]	5a, d, e, f

The target cartridge itself was not analyzed, but the power that is generated in the cartridge that was not included in the rod heat dissipation has been added uniformly to the average rod powers, to account for heating of the cooling water. For the current design this heating is estimated to be [redacted] W per cartridge (30441R00031). 5a, d, e, f Also note that the rod with the peak linear power is located in the middle of the cartridge, whereas the rod with the highest total power is located at the end of the cartridge. Besides their different heating rates, these rods will experience different cooling rates due to their different locations in the cartridge. So, both need to be analyzed. Table 2 shows the essential geometric parameters, and their variations, for the rods and cartridge.

[redacted]

Table 2
Rod and Cassette Geometry and Their Variations

Parameter	Minimum	Nominal	Maximum	
Pellet OD, mm (5.0)		5.0000		5a, b, f
Helium gap, mm		0.0500		
Cladding ID, mm (5.1)		5.100		
Cladding thickness, mm (0.5 +0.15/-0.0)		0.500		
Cladding OD, mm		6.100		
Pellet/Zircaloy gap, µm		50.00		
Scallop diameter, mm (14.45)		14.450		
Rod pitch, mm (11.6332)		11.633		
11 Rod cartridge flow area, mm^2		1318.066		5a, b, f
11 Rod wetted perimeter, mm		526.639		
Average cartridge hydraulic diameter, mm		10.011		
Flow area per rod, in mid-cartridge, mm^2		118.330		5a, b, f
Wetted perimeter per rod, in mid-interior, mm		46.208		
Rod hydraulic diameter, in cartridge interior, mm		10.243		
Flow area per rod, at cartridge end, mm^2		126.549		5a, b, f
Wetted perimeter per rod, at cartridge end, mm		55.384		
Rod hydraulic diameter, at cartridge end, mm		9.140		

Dimensions of the target assembly pellet and cladding are specified in 30441D00211 and 30441D00207. Each of the two target cartridges has an active, nominal heated length of 600 mm, consisting of 11 rods filled with 5.0 mm UO_2 pellets. The pellets are clad in Zircaloy-4 tubes, with an ID of 5.1 mm and a thickness of 0.5 mm . As Table 2 shows, this results in a nominal gap 50 µm, with a maximum and minimum gap size of respectively. The smallest gap increases the conduction heat transfer through the gap, resulting in the coldest UO_2. Conversely, the largest gap decreases the conductive heat transfer though the gap, resulting in the hottest UO_2. In keeping with this, the small gap analysis case shall also use the minimum cladding thickness consistent with the Zircaloy ID, while the large gap analyses shall use the maximum cladding thicknesses. 5a, b, f

Each pellet will be dished and chamfered on its ends to facilitate assembly and mitigate in situ thermal expansion stresses. It also reduces inter-pellet axial conduction. This small reduction in pellet volume will also serve to slightly reduce the amount of heat generated in the pellet. This reduction in heat generation was conservatively neglected in these analyses which used the full cylindrical volume of each pellet.

The pellet/clad gap is filled with He, which will be at 1 atm pressure when cold. Above each rod there is a small, 3.5 cm high plenum into which this helium can expand when it is heated, to reduce the gap pressure increase as it heats up. The bulk average temperature of the hot helium in the gap and top plenum was assumed to be 50°C, which is just a little hotter than the temperature of the helium in the 3.5 cm plenum. It should be noted that this assumption simply sets the annular gap pressure of the helium for property calculations, and that the thermal conductance through this gap is a very weak function of this pressure.

The analyses were performed assuming a 1 day burnup rate at the heat rate experienced for the maximum power density pellet in the rod being analyzed. For example, the burnup rate for 1 day, for a 95% dense UO_2 pellet of volume V m^3, with an atomic weight ratio to pure uranium of 1.134, with a density of 10405.79 kg/m^3 and with a heat rate of [redacted], for the pellet with the peak linear power, in terms of pure uranium is:

5a, d, e, f

$$\frac{[redacted]}{10405.79\ kgUO_2/m^3} * 1\ day * \frac{1\ GW}{10^9 W} * \frac{1000\ kgU}{MTU} * \frac{1.134\ kgUO_2}{kgU} = [redacted]\ \frac{GWdays}{MTU}$$

Greater burnup rates increase the relocation cracks in the fuel, and hence the pellet size, with a resultant reduction in the pellet/clad gap, which results in colder UO_2 temperatures. It has no effect on the safety critical temperatures and heat fluxes of the Zircaloy and water.

The thermal model used was one dimensional (radial), and it ignored the effects of axial conduction away from the point of analysis, again conservatively maximizing the predicted temperatures. The pellet shape already minimizes inter-pellet conduction. However, this assumption will maximize the predicted radial heat fluxes at the Zircaloy surface, and thus assure conservative results.

4 METHOD

The intra-rod distribution of the fission heating of the assembly of 30441R00031 was examined. As shown in Table 1, the pellet with the peak linear heat rate ([redacted]) has that peak heat rate at approximately 30% of the rod length above the coolant entrance, at a point where 35.4% of the total rod heat has been generated. These analyses were, therefore, performed for that maximum heat generation rate, at the water temperature with a 35.4% total temperature rise and a 30% total rod pressure drop. For the maximum power rod, the peak

5a, d, e, f

[redacted]

heat generation rate is where the water temperature has a 45.3% total temperature rise and a 42% total rod pressure drop.

The heat generated radially in the UO_2 pellet itself was based on the self-shielding analysis of Reference 4. The normalized local heat rate used was:

$$Q_{norm} = 1.33305x10^{-4}r^4 - 2.48001x10^{-5}r^3$$

$$+ 2.15986x10^{-2}r^2 - 1.02088x10^{-5}r + 9.30941x10^{-1}$$

where r is the local pellet radius in mm, 0 - 2.5, and
Q_{norm} is the local normalized generation heat rate fraction that should be multiplied by the pellet average heat rate to get the local heat rate

This is shown in Figure 2

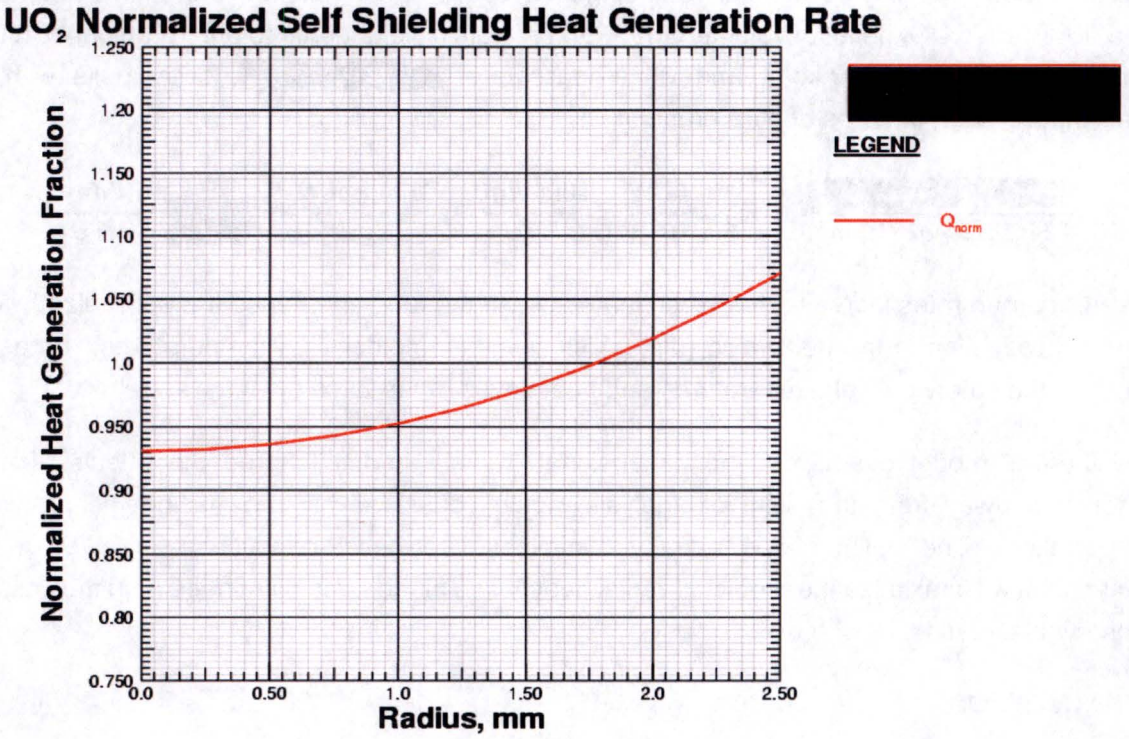

Figure 2. Normalized UO_2 heat generation as a function of pellet radius

[redacted]

Properties of UO_2 (Ref. 5) and Zircaloy-4 (Ref. 4) are shown in Figure 3 and Figure 4.

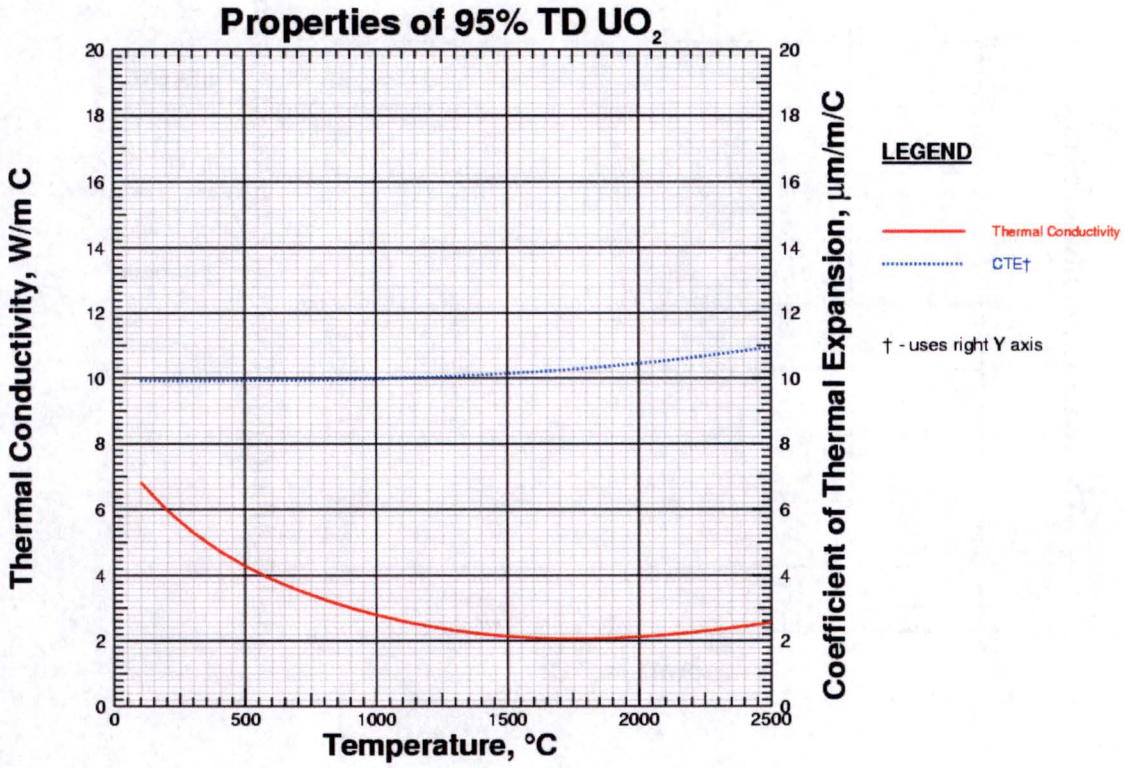

Figure 3. UO_2 thermal conductivity and thermal expansion coefficient for 95% theoretical density

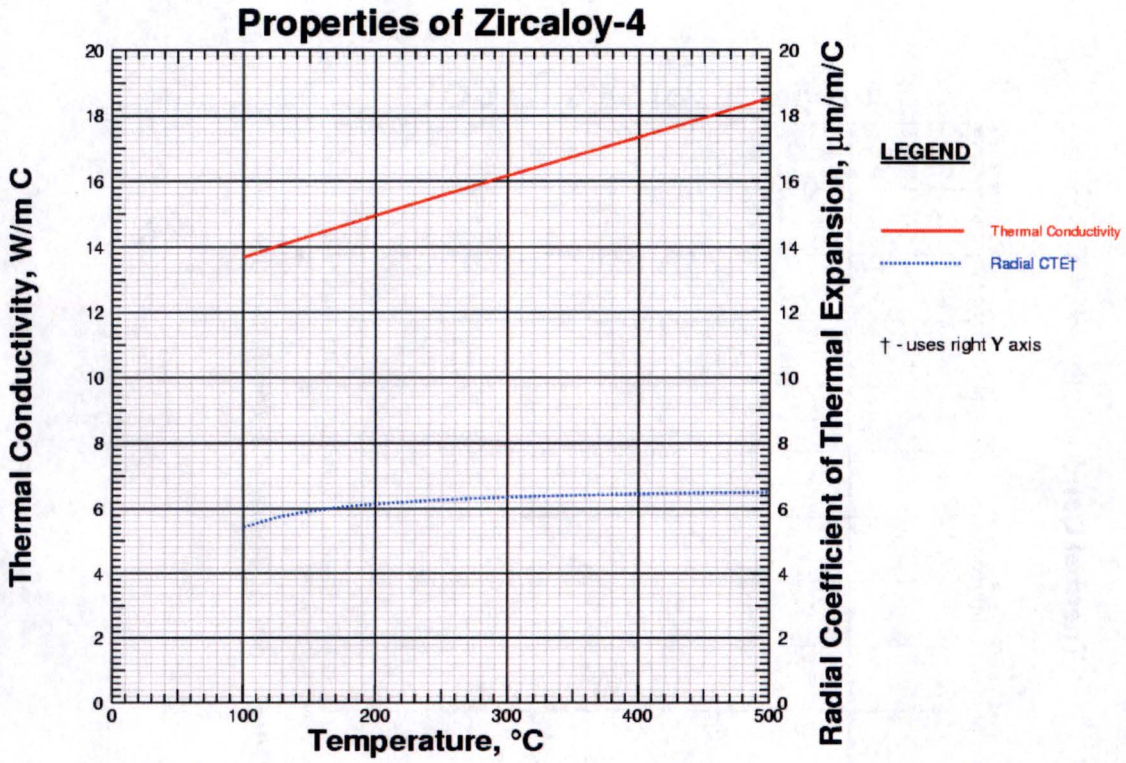

Figure 4. The thermal conductivity and radial thermal expansion coefficient for Zircaloy-4

Typical helium thermal conductivities are shown in Figure 5. The base thermal conductivity and all other properties of the helium in the pellet/cladding gaps were calculated using NIST REFPROP9 data (Ref. 6), and then corrected for the behavior of a gas in a small gap due to wall effects (Ref. 7). The accommodation coefficient used in the small gap conduction equation was 0.38 (Ref. 8). (Although shown in the figure at a typical 2 atm pressure, actual instantaneous temperature dependent pressures, as well as gap sizes, were used in the calculations.) Although conduction through the helium dominates the heat transfer between the UO_2 and Zircaloy, thermal radiation across the gap was also included in the model.

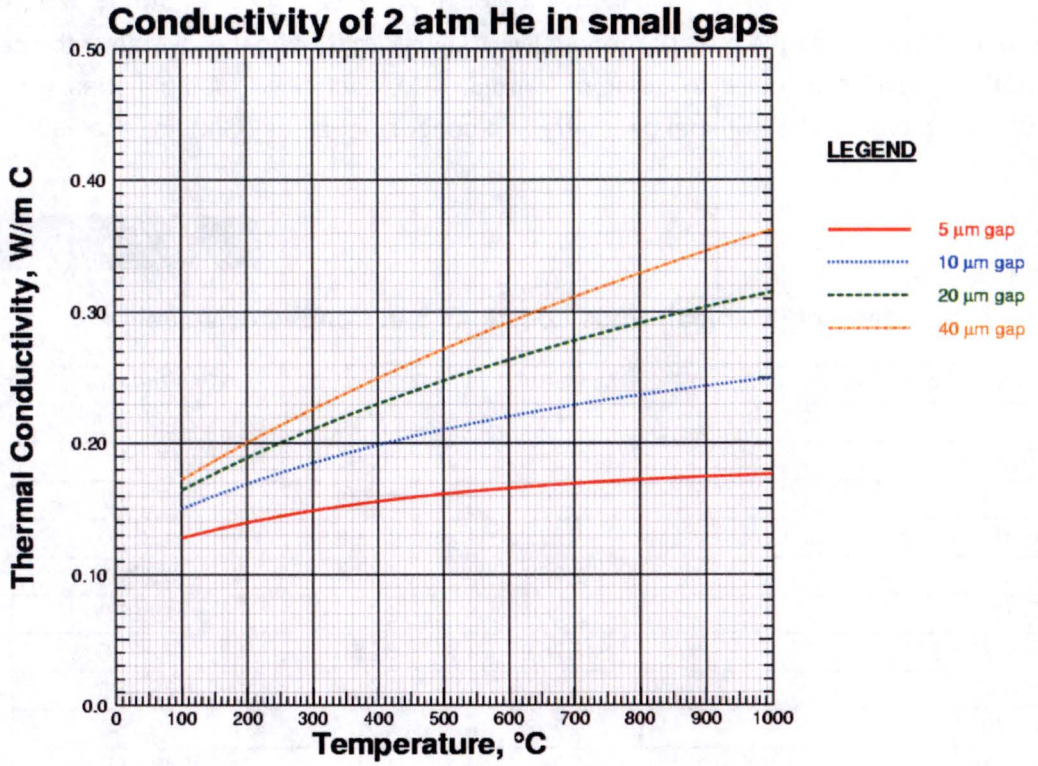

Figure 5. The thermal conductivity of helium (2 atm pressure used as an example)

A finite difference program, SINDA (Ref. 9) was used to analyze the assembly. 30441R00029 provides the software verification test report for SINDA.

A "worst case" rod (which was either the rod with the peak local heat flux or the rod with the maximum total power was modelled using ten (10) concentric rings of UO_2 conductors (labeled U1-U10 in the table, below), each with their own temperature dependent thermal conductivity, connected between their geometric centers by conductances accounting for the expanding cylindrical geometry of the rings:

$$Q = G * \Delta T$$

$$G = \frac{2\pi kl}{\ln\left(\frac{R_o}{R_i}\right)}$$

[redacted]

where Q is heat in watts, T is temperature in °C, and G is the temperature dependent thermal conductance of the material. In cylindrical coordinates, it is the product of 2 * π, the axial length of the cylinder (L, in meters), the material conductivity (k, in W/m C), and the inverse of the natural logarithm of the cylindrical outer to inner radii ratio. Conductances of the nodes (at room temperature) locations for the nominal geometry and conductor values (G/k) are shown in Table 3.

[redacted]

Table 3
Summary of (Nominal) Node Locations and Conductor Values

Conduction Conductors	Conductor D_i	Conductor D_o	$G/k=2\pi/\ln(D_o/D_i)$
	mm	Mm	(k=W/m C)
U1 - U2	0.354	0.791	4.685
U2 - U3	0.791	1.275	7.891
U3 - U4	1.275	1.768	11.530
U4 - U5	1.768	2.264	15.241
U5 - U6	2.264	2.761	18.978
U6 - U7	2.761	3.260	22.726
U7 -U8	3.260	3.758	26.480
U8 - U9	3.758	4.257	30.238
U9 - U10	4.257	4.757	33.999
U10 - U10 Surface	4.757	5.000	75.534

All other conductors are calculated iteratively, as their geometry changes as a function of their thermal expansion, which is a function of their temperature. In addition, radiation heat transfer was modeled across the helium gap, between the UO_2 and Zircaloy, assuming a UO_2 emissivity of 0.6 (Ref. 5) and a Zircaloy emissivity of 0.625 (Ref.4).

In addition to a nominal safety margin of 10% on heat transfer coefficients, several additional margins were included in these analyses to account for operating uncertainties were included in these analyses. These margins are based on typical instrumentation measurement uncertainties. The pressure drops through the entire target assembly were calculated using the ANSYS FLUENT CFD program (30441R00038). These pressure drops were *reduced* by 5% for the thermal analyses. Normally, pressure drops are *increased* by a margin to add conservativeness to calculations. In this case, however, local system pressures are determined by the known assembly outlet pressure, which is set by the depth of the assembly in the pool. Pressures within the cartridge are calculated as that outlet pressure plus the pressure drop to the outlet. Therefore a higher pressure drop will result in a higher pressure within the assembly.

[redacted]

As the saturation temperature of water increases with pressure, higher internal assembly pressures will result in higher (less conservative) predicted critical heat flux ratios, which, therefore, dictates using a reduced pressure drop. Also, an uncertainty of 2°C (3.6°F) was applied to the "known" system boundary condition of system inlet temperature, and of 5% on the system flow rate, to account for possible errors in measuring these critical operating parameters. The local inlet temperature was increased by this margin, while the flow rate was decreased. As with the pressure drop reduction allowance, the effect of these changes is also to reduce the calculated critical heat flux, further increasing the safety margins in the analyses.

As indicated above, the pressure drops through the Target Assembly were calculated in 30441R00038. At nominal flow there will be a 13.62 psid pressure drop through the assembly; [redacted] will be across the inlet rod assembly support grid; [redacted] will be across the rods, and [redacted] will be between the top of the rods and the assembly exit. The pressure at the assembly exit will be 24.37 psi, the pressure in the pool of 102°F water, 6.85 m deep. 5a, d, e, f

Water-to-tube heat transfer coefficients were calculated for the assembly using turbulent annular correlations from Dirker and Meyer (Ref. 12). These were then used to calculate the hot Zircaloy wall surface temperature. This wall temperature was then compared to a value equal to the sum of the local saturation temperature of water and the amount of wall superheat required to boil the water in the subcooled nucleate boiling regime, as proposed by Jens-Lottes (Ref. 13). If the calculated wall temperature was less than this value, the calculations proceeded normally as a single phase liquid cooling. If, however, the predicted wall temperature exceeded the Jens-Lottes threshold value, the wall temperature was set to be the Jens-Lottes boiling temperature, with the coolant immediately at the wall being at the local water saturation temperature. (Heat transfer coefficients reported herein were adjusted to reflect the calculations as if they were made between the wall and the bulk water, not saturation at the wall temperatures.) The critical heat flux, and the Critical Heat Flux Ratio were then calculated using correlations from Bernath (Ref. 14), Macbeth (Ref. 15) and Groeneveld (Ref. 16). As long as these CHFR's are all greater than 2, there will be a 100% safety margin, ensuring that any boiling that takes place will be in the subcooled nucleate boiling regime, and that the Jens-Lottes correlation, therefore, is applicable, and the calculations can proceed without the possibility that a dryout failure will occur. The 100% safety factor on the critical heat flux is meant to cover all of (and only) the uncertainties in the critical heat flux calculation (the data scatter in the Bernath, Macbeth and Groeneveld correlations). The local heat flux calculations (and hence, the Critical Heat Flux Ratio), already have the compensation for the uncertainties of the system itself built into them by the margins imposed in the calculations.

Figure 6 shows the effect of the changing axial heat flux and coolant temperature on the CHFR calculations for both the peak linear power (PLP) rod and the maximum heating (MH) rod.

[redacted]

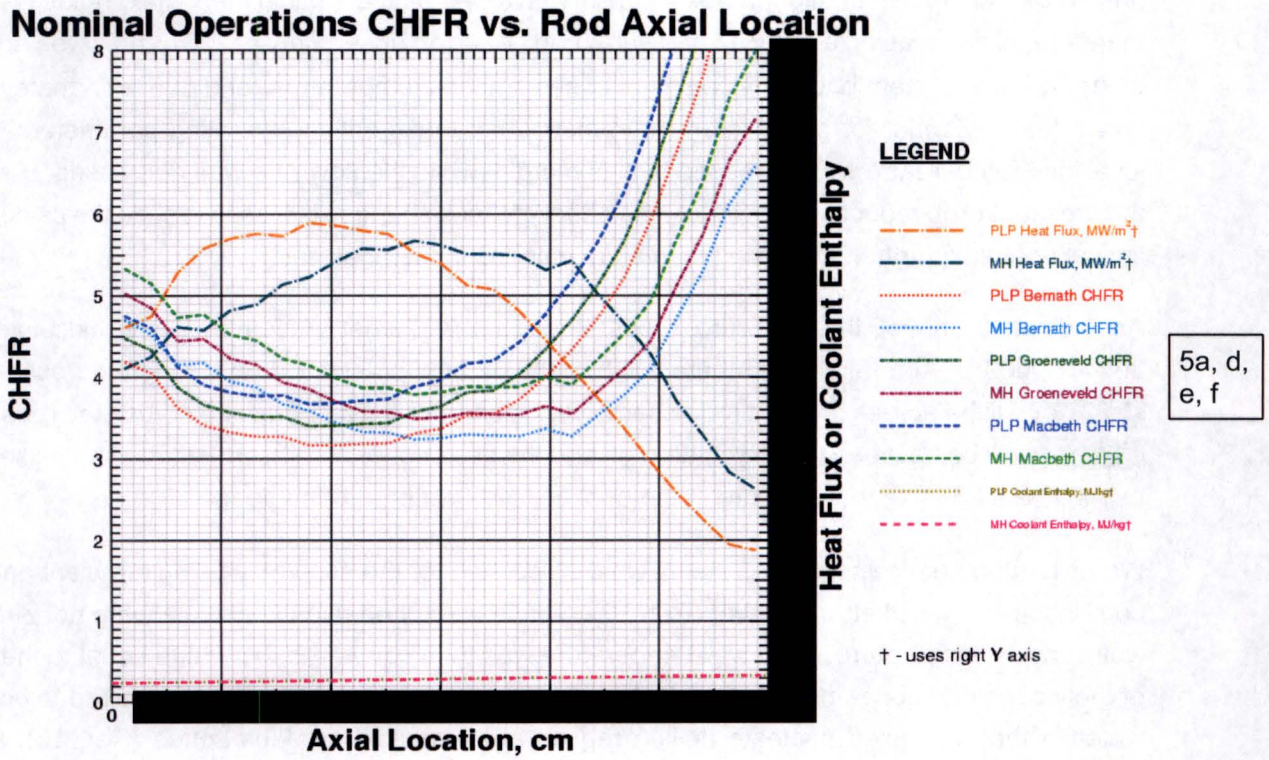

5a, d, e, f

Figure 6. Effect of axial location on heat flux and CHFR

The red dotted line shows the CHRF (Bernath) for the peak linear power rod. The blue dotted line shows the CHFR (Bernath) for the maximum power rod. (In all these analyses, the Bernath CHFR was consistently the lowest and most conservative CHFR calculated.) Note that although the point of maximum heat flux occurs at different points along the rod for the PLP and MH cases, the minimum CHFR is almost the same for both cases. Note, too, that small temperature rise of the coolant yields an almost constant line for the coolant enthalpy as a function of rod axial (the two, overlapping lines at the bottom of the plot). Thus the point of the minimum critical heat flux ratio coincides with the location of the maximum heat flux in the rod. As indicated previously, both rods were analyzed for all scenarios considered to ensure the absolute minimum CHFR was predicted.

For each analysis, the Coefficients of Thermal Expansion of the UO_2 and the Zircaloy were iteratively calculated and the expansion at the current temperature was calculated. Given that expansion rate, the current gap geometry was calculated, and the conductivity of the helium through the gap at its current temperature and size was calculated. The entire temperature field

was then recalculated. This was repeated until no change in temperature (and hence, gap) was seen.

The nominal water inlet and outlet temperatures of 28.89°C (84°F) and 38.89°C (102°F), at a pool temperature of 38.89°C (102°F), assume that there will be 11 active rods in the cartridge, each dissipating an average of [redacted]. However, varying operational scenarios require that rod counts below 11 may be used, with the minimum number of rods that may be placed in a cartridge being 3. (Note that there is only one common coolant source for both target assemblies. This implies that there is only one possible inlet temperature for both assemblies, and hence, the rod count in each assembly must be the same.) To operate with less than 11 active rods, while maintaining the same flow characteristics and mixed target outlet temperature, in addition to the normal UO_2 filled rods, the balance of the cartridge shall be filled with non-fissioning/non-heat generating rods, and the target coolant inlet temperature shall be adjusted accordingly, while maintaining the same overall coolant flow rate. As water shall exit the non-heat generating rod annuli at essentially the same temperature as it enters (there being a very small amount of gamma and cartridge heating), but leave the heated rod annuli 10°C hotter (for an average rod) than it enters, the mixed outlet temperature for n active rods is (with all temperatures in °C):

5a, d, e, f

$$T_{out_{mixed}} = T_{pool} = \frac{n * (T_{inlet} + 10) + (11 - n) * T_{inlet}}{11}$$

$$T_{inlet} = T_{pool} - 0.9091 * n$$

Table 4 shows the variation in coolant temperatures as the active rod count varies.

[redacted]

Table 4
Variation of Coolant Inlet Temperature with Active Rod Count

Active Rods	Non Heating Rods	T_{in} °C	T_{in} °F	T_{out} °C	T_{out} °	Mixed T_{out} °C	Mixed T_{out} °F
1*	10	37.98	100.36	47.98	118.36	38.89	102.00
3	8	36.16	97.09	46.16	115.09	38.89	102.00
4	7	35.25	95.46	45.25	113.46	38.89	102.00
5	6	34.34	93.82	44.34	111.82	38.89	102.00
6	5	33.44	92.18	43.44	110.18	38.89	102.00
7	4	32.53	90.55	42.53	108.55	38.89	102.00
8	3	31.62	88.91	41.62	106.91	38.89	102.00
9	2	30.71	87.27	40.71	105.27	38.89	102.00
10	1	29.80	85.64	39.80	103.64	38.89	102.00
11	0	28.89	84.00	38.89	102.00	38.89	102.00

* Operations with only 1 active rod are allowable only for system commissioning testing as this will result in CHFRs below 2 at maximum power/minimum flow conditions.

Thus, for example, to achieve a mixed outlet cartridge temperature equal to a nominal pool temperature of 38.89°C (102°F): For 11 active rods, T_{inlet} = 28.89°C (84°F); For 3 active rods it is 36.16°C (97.09°F). For each additional degree of initial temperature of the pool, the cartridge inlet temperature will need to increase by the same number of degrees. For these analyses, it was assumed that 3 rod operations would not occur if the pool temperature exceeded 42.22°C (108°F), as these conditions would allow the CHFR to fall below 2.0. As both the inlet and outlet coolant temperatures rise with decreasing active rod counts, the most severe operating conditions are those with the least active rods.

[redacted]

5 SUMMARY RESULTS AND CONCLUSION

Analyses were performed for a full matrix of possible operating conditions, varying reactor power (10.0 and 11.5 MWt), coolant flow (100% and 85%), UO_2/Cladding gap (50 µm nominal, [redacted] minimum, [redacted] maximum), active rod count (11 maximum, 3 minimum), rod type (peak linear power and maximum heat) and operational margin (nominal and extra). A full complement of the nominal gap results with both 3 and 11 rods is shown here. In addition, the worst case (lowest CHFR) runs are also shown. These are those cases with only 3 rods, the smallest UO_2/Cladding gap and the largest possible water flow channel diameter.

5a, b, f

Figure 7 shows a typical cross section of the temperatures through the target rod and surrounding coolant at its hottest point. It is for nominal operations at 10 MWt reactor power, 100% flow, with 11 rods for the rod with the peak linear power, with all nominal dimensions and no added calculational margin. The UO_2 goes from 2000°C at its center to 425°C at its outside radius at 2.5 mm. There will be about a 160°C temperature drop across the helium UO_2-Zircaloy gap to 263°C at the Zircaloy ID, and another 100°C to the Zircaloy OD, which will be at 156°C. This is the temperature set by the water boiling at it surface. The bulk water away from the surface will be 32°C.

[redacted]

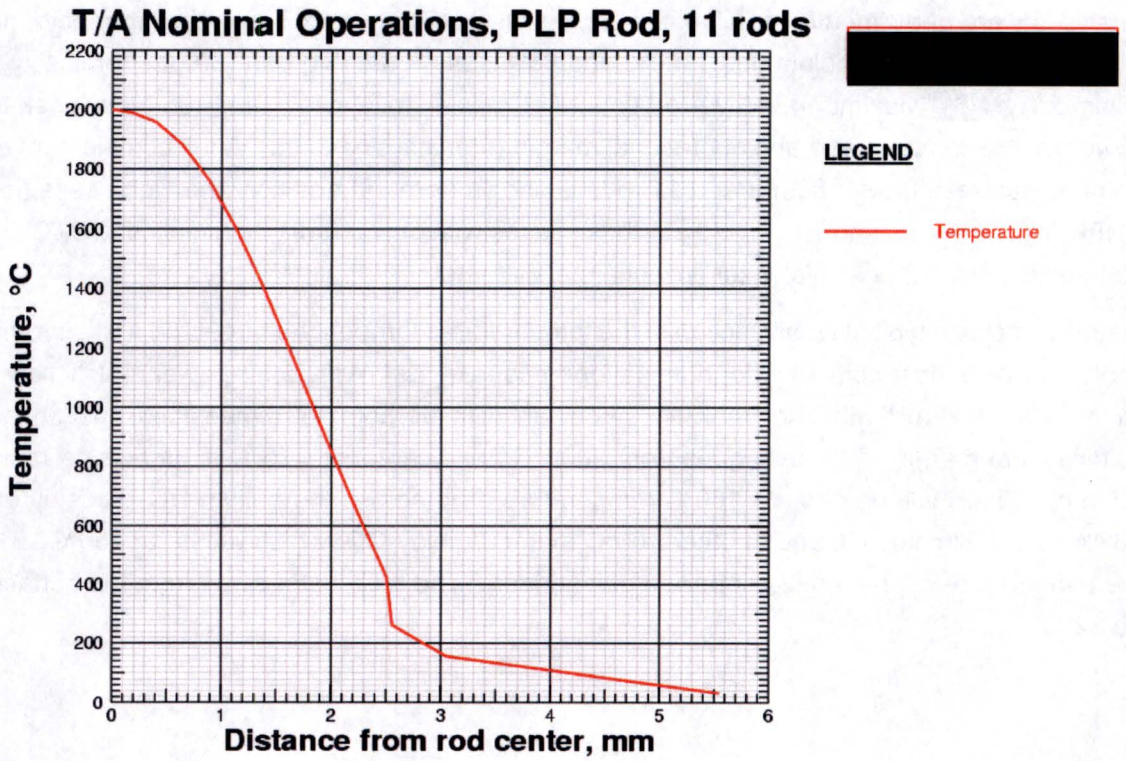

Figure 7. Temperature cross section at nominal operations

As mentioned previously, steady state analyses were performed for all combinations of minimum, nominal and maximum rod/cladding gaps, minimum, nominal and maximum scallop diameter, rod type and location (peak power at mid-cartridge and maximum power at the end of the cartridge), and rod count. All analyses predicted UO_2 temperatures well below the 2400°C limit, as well as CHFRs in excess of 2.0. Based on CHFRs, of all the analyses, 3 rod cases (with higher water cartridge inlet temperatures than their 11 rod counterparts) were always worse than 11; minimum gap cases CHFRs were always lower than the others; maximum water channel dimension CHFRs were always worse than smaller ones. The peak power rod CHFRs were always very similar to that of the maximum average power rod. (The actual minimum CHFR for various cases was sometimes in the peak power rod, and at other times in the maximum heating rod. Thus both rod scenarios were always analyzed.) Table 5 shows the details of steady state operations for an 11 rod target, for both the nominal conditions, and for the worst case analyzed (with additional calculation margins), for both the peak power and maximum heating rods at 10 MW reactor power with 100% flow. Table 6 shows the details of those same cases but at 11.5 MWt reactor power and 85% flow, the worst possible case (as the reactor will SCRAM at either higher power or lower

[redacted]

flow). Tables 7 and 8 show the equivalent 3 rod cases. Table 9 shows the worst (lowest CHFR) cases, those being for 3 rods, with a [redacted] gap and added calculational margin. 5a, b, f

Table 5
Details of 11 Nominal Rod Target Operations at 10 MWt Reactor Power, 100% Flow

[redacted]	Peak Power Rod No added Margin	Peak Power Rod Maximum added Margin	Maximum Heating Rod No added Margin	Maximum Heating Rod Maximum added Margin
Reactor power, MWt	10	10	10	10
Flow %	100	100	100	100
Active rods	11	11	11	11
Pool temperature, °C	38.9	40.9	38.9	40.9
Target inlet temperature, °C	28.9	30.9	28.9	30.9
Cold gap	Nominal	Nominal	Nominal	Nominal
Rod type	Peak Linear	Peak Linear	Max Heating	Max Heating
Rod location	Middle	Middle	End	End
Added error margin	None	Maximum	None	Maximum
Scallop diameter	Nominal	Maximum	Nominal	Maximum
Cold gap, µm	50	50	50	50
UO_2 radial growth, µm	40.06	40.01	38.7	38.66
Cladding radial growth, µm	2.92	2.9	2.88	2.86
Relocation growth, µm	5.11	5.11	4.94	4.94
Hot gap, µm	7.76	7.79	9.24	9.26
Helium gap pressure, atm	1.74	1.74	1.71	1.71
Plenum height, mm (Cold)	35	35	35	35
Plenum height, mm (Hot)	32.61	32.61	32.55	32.56
		(Cont'd)		
Axial CTE UO_2, µm/(m°C)	9.87	9.87	9.87	9.87
Radial CTE UO_2, µm/(m°C)	10.47	10.47	10.44	10.44
Radial CTE Zircaloy, µm/(m°C)	6.17	6.16	6.16	6.16
UO_2 centerline temperature, °C	2000.1	1998.7	1942.4	1941.1
UO_2 average temperature, °C	1117	1115.8	1097.4	1096.4
UO_2 surface temperature, °C	423.6	422.9	433.0	432.4
Helium temperature, °C	345.2	344.2	348.1	347.2

[redacted]

Table 5
Details of 11 Nominal Rod Target Operations at 10 MWt Reactor Power, 100% Flow

[redacted]	Peak Power Rod No added Margin	Peak Power Rod Maximum added Margin	Maximum Heating Rod No added Margin	Maximum Heating Rod Maximum added Margin	
Cladding temperature at ID, °C	263.0	261.8	258.4	257.2	
Mean cladding temperature, °C	206.0	204.7	203.4	202.2	
Cladding temperature at OD, °C	156.1	154.8	155.4	154.1	
UO_2 gap conductance, W/(m^2 C)	22160.5	22092.4	19603.2	19539.5	
Coolant HTC, W/(m^2 C)	[redacted]	[redacted]	[redacted]	[redacted]	5a, d, e, f
Water (scallop) OD, mm	14.45	14.823	14.45	14.823	
D_h, mm	10.243	10.746	9.14	9.555	
Re (D_h)	[redacted]	[redacted]	[redacted]	[redacted]	
Local coolant velocity, m/s	[redacted]	[redacted]	[redacted]	[redacted]	5a, d, e, f
Mass flow per rod, kg/s	[redacted]	[redacted]	[redacted]	[redacted]	
Mass flow per target, kg/s	[redacted]	[redacted]	[redacted]	[redacted]	
Mass flow per target, sgpm	[redacted]	[redacted]	[redacted]	[redacted]	
Coolant inlet temperature, °C	28.89	30.89	28.89	30.89	
Local coolant temperature, °C	32.52	34.71	34.02	36.29	
Coolant outlet temperature, °C	39.14	41.68	39.61	42.17	
Local saturation temperature, °C	124.53	123.15	124.11	122.78	
Peak pellet power density, W/cc	[redacted]	[redacted]	[redacted]	[redacted]	
Heat (modeled) per rod, W	[redacted]	[redacted]	[redacted]	[redacted]	5a, d, e, f
Heat flux at cladding OD, W/m^2	[redacted]	[redacted]	[redacted]	[redacted]	
Bernath CHF, W/m^2	[redacted]	[redacted]	[redacted]	[redacted]	
Bernath CHFR	3.17	2.93	3.18	2.92	
Macbeth CHF, W/m^2	[redacted]	[redacted]	[redacted]	[redacted]	5a, d, e, f
Macbeth CHFR	3.67	3.60	4.06	4.00	
Groeneveld CHF, W/m^2	[redacted]	[redacted]	[redacted]	[redacted]	
Groeneveld CHFR	3.40	3.13	3.50	3.24	
Minimum CHFR	3.167	2.933	3.176	2.924	
Pressure at CHFR, atm	2.2588	2.1645	2.2299	2.1400	

[redacted]

Table 6
Details of 11 Nominal Rod Target Operations at 11.5 MWt Reactor Power, 85% flow

[redacted]	Peak Power Rod No added Margin	Peak Power Rod Maximum added Margin	Maximum Heating Rod No added Margin	Maximum Heating Rod Maximum added Margin
Reactor power, MWt	11.5	11.5	11.5	11.5
Flow %	85	85	85	85
Active rods	11	11	11	11
Pool temperature, °C	38.9	40.9	38.9	40.9
Target inlet temperature, °C	28.9	30.9	28.9	30.9
Cold gap	Nominal	Nominal	Nominal	Nominal
Rod type	Peak Linear	Peak Linear	Max Heating	Max Heating
Rod location	Middle	Middle	End	End
Added error margin	None	Maximum	None	Maximum
Scallop diameter	Nominal	Maximum	Nominal	Maximum
Cold gap, µm	50	50	50	50
UO_2 radial growth, µm	45.16	45.11	43.79	43.75
Cladding radial growth, µm	3.03	3.01	2.98	2.97
Relocation growth, µm	5.11	5.11	4.94	4.94
Hot gap, µm	2.77	2.79	4.25	4.27
Helium gap pressure, atm	1.85	1.85	1.82	1.82
Plenum height, mm (Cold)	35	35	35	35
Plenum height, mm (Hot)	32.87	32.88	32.79	32.79
Axial CTE UO_2, µm/(m°C)	9.86	9.86	9.86	9.86
Radial CTE UO_2, µm/(m°C)	10.57	10.57	10.55	10.55
Radial CTE Zircaloy, µm/(m°C)	6.19	6.18	6.18	6.17
UO_2 centerline temperature, °C	2204.7	2203.6	2150.8	2149.8
UO_2 average temperature, °C	1181.0	1180.0	1165.7	1164.9
UO_2 surface temperature, °C	379.3	378.7	394.2	393.8
Helium temperature, °C	328.5	327.8	333.9	333.2
Cladding temperature at ID, °C	277.2	276.2	272.1	271.2
Mean cladding temperature, °C	212.1	211.1	209.3	208.4
Cladding temperature at OD, °C	154.9	153.9	154.2	153.3
UO_2 gap conductance, W/(m^2 C)	40111.0	39965.3	32241.7	32132

[redacted]

Table 6 (Cont'd)
Details of 11 Nominal Rod Target Operations at 11.5 MWt Reactor Power, 85% flow

[redacted]	Peak Power Rod No added Margin	Peak Power Rod Maximum added Margin	Maximum Heating Rod No added Margin	Maximum Heating Rod Maximum added Margin	
Coolant HTC, W/(m^2 C)	[redacted]	[redacted]	[redacted]	[redacted]	5a, d, e, f
Water (scallop) OD, mm	14.450	14.823	14.450	14.823	
D_h, mm	10.243	10.746	9.140	9.555	
Re (D_h)	[redacted]	[redacted]	[redacted]	[redacted]	
Local coolant velocity, m/s	[redacted]	[redacted]	[redacted]	[redacted]	5a, d, e, f
Mass flow per rod, kg/s	[redacted]	[redacted]	[redacted]	[redacted]	
Mass flow per target, kg/s	[redacted]	[redacted]	[redacted]	[redacted]	
Mass flow per target, sgpm	[redacted]	[redacted]	[redacted]	[redacted]	
Coolant inlet temperature, °C	28.89	30.89	28.89	30.89	
Local coolant temperature, °C	33.81	36.06	35.83	38.19	
Coolant outlet temperature, °C	42.76	45.49	43.39	46.16	
Local saturation temperature, °C	122.06	121.00	121.74	120.73	
Peak pellet power density, W/cc	[redacted]	[redacted]	[redacted]	[redacted]	
Heat (modeled) per rod, W	[redacted]	[redacted]	[redacted]	[redacted]	
Heat flux at cladding OD, W/m^2	[redacted]	[redacted]	[redacted]	[redacted]	5a, d, e, f
Bernath CHF, W/m^2	[redacted]	[redacted]	[redacted]	[redacted]	
Bernath CHFR	2.47	2.31	2.47	2.29	
Macbeth CHF, W/m^2	[redacted]	[redacted]	[redacted]	[redacted]	
Macbeth CHFR	3.24	3.18	3.59	3.53	5a, d, e, f
Groeneveld CHF, W/m^2	[redacted]	[redacted]	[redacted]	[redacted]	
Groeneveld CHFR	2.69	2.51	2.79	2.62	
Minimum CHFR	2.473	2.307	2.465	2.286	
Pressure at CHFR, atm	2.0921	2.0240	2.0712	2.0063	

[redacted]

Table 7
Details of 3 Nominal Rod Target Operations at 10 MWt Reactor Power, 100% Flow

[redacted]	Peak Power Rod No added Margin	Peak Power Rod Maximum added Margin	Maximum Heating Rod No added Margin	Maximum Heating Rod Maximum added Margin
Reactor power, MWt	10	10	10	10
Flow %	100	100	100	100
Active rods	3	3	3	3
Pool temperature, °C	42.2	44.2	42.2	44.2
Target inlet temperature, °C	39.5	41.5	39.5	41.5
Cold gap	Nominal	Nominal	Nominal	Nominal
Rod type	Peak Linear	Peak Linear	Max Heating	Max Heating
Rod location	Middle	Middle	End	End
Added error margin	None	Maximum	None	Maximum
Scallop diameter	Nominal	Maximum	Nominal	Maximum
Cold gap, µm	50	50	50	50
UO_2 radial growth, µm	40.06	40.01	38.7	38.66
Cladding radial growth, µm	2.92	2.9	2.88	2.86
Relocation growth, µm	5.11	5.11	4.94	4.94
Hot gap, µm	7.76	7.79	9.24	9.26
Helium gap pressure, atm	1.74	1.74	1.71	1.71
Plenum height, mm (Cold)	35	35	35	35
Plenum height, mm (Hot)	32.61	32.61	32.55	32.56
Axial CTE UO_2, µm/(m°C)	9.87	9.87	9.87	9.87
Radial CTE UO_2, µm/(m°C)	10.47	10.47	10.44	10.44
Radial CTE Zircaloy, µm/(m°C)	6.17	6.16	6.16	6.16
UO_2 centerline temperature, °C	2000.1	1998.7	1942.4	1941.1
UO_2 average temperature, °C	1117	1115.8	1097.4	1096.4
UO_2 surface temperature, °C	423.6	422.9	433	432.4
Helium temperature, °C	345.2	344.2	348.1	347.2
Cladding temperature at ID, °C	263	261.8	258.4	257.2
Mean cladding temperature, °C	206	204.7	203.4	202.2
Cladding temperature at OD, °C	156.1	154.8	155.4	154.1
UO_2 gap conductance, W/(m^2 C)	22160.5	22092.4	19603.2	19539.5

[redacted]

Table 7 (Cont'd)
Details of 3 Nominal Rod Target Operations at 10 MWt Reactor Power, 100% Flow

[redacted]	Peak Power Rod No added Margin	Peak Power Rod Maximum added Margin	Maximum Heating Rod No added Margin	Maximum Heating Rod Maximum added Margin	
Coolant HTC, W/(m^2 C)	[redacted]	[redacted]	[redacted]	[redacted]	5a, d, e, f
Water (scallop) OD, mm	14.450	14.823	14.450	14.823	
D_h, mm	10.243	10.746	9.140	9.555	
Re (D_h)	[redacted]	[redacted]	[redacted]	[redacted]	
Local coolant velocity, m/s	[redacted]	[redacted]	[redacted]	[redacted]	5a, d, e, f
Mass flow per rod, kg/s	[redacted]	[redacted]	[redacted]	[redacted]	
Mass flow per target, kg/s	[redacted]	[redacted]	[redacted]	[redacted]	
Mass flow per target, sgpm	[redacted]	[redacted]	[redacted]	[redacted]	
Coolant inlet temperature, °C	39.49	41.49	39.49	41.49	
Local coolant temperature, °C	43.12	45.31	44.62	46.89	
Coolant outlet temperature, °C	49.74	52.28	50.21	52.77	
Local saturation temperature, °C	124.53	123.15	124.11	122.78	
Peak pellet power density, W/cc	[redacted]	[redacted]	[redacted]	[redacted]	
Heat (modeled) per rod, W	[redacted]	[redacted]	[redacted]	[redacted]	5a, d, e, f
Heat flux at cladding OD, W/m^2	[redacted]	[redacted]	[redacted]	[redacted]	
Bernath CHF, W/m^2	[redacted]	[redacted]	[redacted]	[redacted]	
Bernath CHFR	2.90	2.68	2.91	2.67	
Macbeth CHF, W/m^2	[redacted]	[redacted]	[redacted]	[redacted]	
Macbeth CHFR	3.53	3.47	3.91	3.85	5a, d, e, f
Groeneveld CHF, W/m^2	[redacted]	[redacted]	[redacted]	[redacted]	
Groeneveld CHFR	3.16	2.91	3.26	3.02	
Minimum CHFR	2.905	2.683	2.909	2.671	
Pressure at CHFR, atm	2.2588	2.1645	2.2299	2.1400	

[redacted]

Table 8
Details of 3 Nominal Rod Target Operations at 11.5 MWt Reactor Power, 85% Flow

[redacted]	Peak Power Rod No added Margin	Peak Power Rod Maximum added Margin	Maximum Heating Rod No added Margin	Maximum Heating Rod Maximum added Margin
Reactor power, MWt	11.5	11.5	11.5	11.5
Flow %	85	85	85	85
Active rods	3	3	3	3
Pool temperature, °C	42.2	44.2	42.2	44.2
Target inlet temperature, °C	39.5	41.5	39.5	41.5
Cold gap	Nominal	Nominal	Nominal	Nominal
Rod type	Peak Linear	Max Heating	Max Heating	Max Heating
Rod location	Middle	End	End	End
Added error margin	None	Maximum	None	Maximum
Scallop diameter	Nominal	Maximum	Nominal	Maximum
Cold gap, µm	50	50	50	50
UO_2 radial growth, µm	45.16	43.75	43.79	43.75
Cladding radial growth, µm	3.03	2.97	2.98	2.97
Relocation growth, µm	5.11	4.94	4.94	4.94
Hot gap, µm	2.77	4.27	4.25	4.27
Helium gap pressure, atm	1.85	1.82	1.82	1.82
Plenum height, mm (Cold)	35	35	35	35
Plenum height, mm (Hot)	32.87	32.79	32.79	32.79
Axial CTE UO_2, µm/(m°C)	9.86	9.86	9.86	9.86
Radial CTE UO_2, µm/(m°C)	10.57	10.55	10.55	10.55
Radial CTE Zircaloy, µm/(m°C)	6.19	6.17	6.18	6.17
UO_2 centerline temperature, °C	2204.7	2149.8	2150.8	2149.8
UO_2 average temperature, °C	1181.0	1164.9	1165.7	1164.9
UO_2 surface temperature, °C	379.3	393.8	394.2	393.8
Helium temperature, °C	328.5	333.2	333.9	333.2
Cladding temperature at ID, °C	277.2	271.2	272.1	271.2
Mean cladding temperature, °C	212.1	208.4	209.3	208.4
Cladding temperature at OD, °C	154.9	153.3	154.2	153.3

[redacted]

Table 8 (Cont'd)
Details of 3 Nominal Rod Target Operations at 11.5 MWt Reactor Power, 85% Flow

[redacted]	Peak Power Rod No added Margin	Peak Power Rod Maximum added Margin	Maximum Heating Rod No added Margin	Maximum Heating Rod Maximum added Margin	
UO_2 gap conductance, W/(m^2 C)	40111.0	32132.0	32241.7	32132.0	
Coolant HTC, W/(m^2 C)	[redacted]	[redacted]	[redacted]	[redacted]	5a, d, e, f
Water (scallop) OD, mm	14.450	14.823	14.450	14.823	
D_h, mm	10.243	9.555	9.140	9.555	
Re (D_h)	[redacted]	[redacted]	[redacted]	[redacted]	
Local coolant velocity, m/s	[redacted]	[redacted]	[redacted]	[redacted]	
Mass flow per rod, kg/s	[redacted]	[redacted]	[redacted]	[redacted]	5a, d, e, f
Mass flow per target, kg/s	[redacted]	[redacted]	[redacted]	[redacted]	
Mass flow per target, sgpm	[redacted]	[redacted]	[redacted]	[redacted]	
Coolant inlet temperature, °C	39.49	41.49	39.49	41.49	
Local coolant temperature, °C	44.40	48.79	46.43	48.79	
Coolant outlet temperature, °C	53.36	56.75	53.99	56.75	
Local saturation temperature, °C	122.06	120.73	121.74	120.73	
Peak pellet power density, W/cc	[redacted]	[redacted]	[redacted]	[redacted]	
Heat (modeled) per rod, W	[redacted]	[redacted]	[redacted]	[redacted]	
Heat flux at cladding OD, W/m^2	[redacted]	[redacted]	[redacted]	[redacted]	5a, d, e, f
Bernath CHF, W/m^2	[redacted]	[redacted]	[redacted]	[redacted]	
Bernath CHFR	2.26	2.08	2.25	2.08	
Macbeth CHF, W/m^2	[redacted]	[redacted]	[redacted]	[redacted]	
Macbeth CHFR	3.13	3.41	3.46	3.41	5a, d, e, f
Groeneveld CHF, W/m^2	[redacted]	[redacted]	[redacted]	[redacted]	
Groeneveld CHFR	2.50	2.45	2.60	2.45	
Minimum CHFR	2.261	2.080	2.250	2.080	
Pressure at CHFR, atm	2.0921	2.0063	2.0712	2.0063	

[redacted]

Table 9
Details of 3 Rod Worst Case Target Operations

[redacted]	Peak Power Rod No added Margin	Peak Power Rod Maximum added Margin	Maximum Heating Rod No added Margin	Maximum Heating Rod Maximum added Margin
Reactor power, MWt	10	10	11.5	11.5
Flow %	100	100	85	85
Active rods	3	3	3	3
Pool temperature, °C	44.2	44.2	44.2	44.2
Target inlet temperature, °C	41.5	41.5	41.5	41.5
Cold gap	Minimum	Minimum	Minimum	Minimum
Rod type	Peak Linear	Max Heating	Peak Linear	Max Heating
Rod location	Middle	End	Middle	End
Added error margin	Maximum	Maximum	Maximum	Maximum
Scallop diameter	Maximum	Maximum	Maximum	Maximum
Cold gap, µm	[redacted]	[redacted]	[redacted]	[redacted]
UO_2 radial growth, µm	[redacted]	[redacted]	[redacted]	[redacted]
Cladding radial growth, µm	[redacted]	[redacted]	[redacted]	[redacted]
Relocation growth, µm	[redacted]	[redacted]	[redacted]	[redacted]
Hot gap, µm	[redacted]	[redacted]	[redacted]	[redacted]
Helium gap pressure, atm	1.66	1.64	1.70	1.70
Plenum height, mm (Cold)	35	35	35	35
Plenum height, mm (Hot)	33.14	33.07	32.99	33.04
Axial CTE UO_2, µm/(m°C)	9.85	9.86	9.86	9.86
Radial CTE UO_2, µm/(m°C)	10.26	10.25	10.52	10.44
Radial CTE Zircaloy, µm/(m°C)	6.17	6.16	6.18	6.18
UO_2 centerline temperature, °C	1796.6	1746.0	2169.9	2061.7
UO_2 average temperature, °C	964.5	952.2	1149.8	1093.4
UO_2 surface temperature, °C	334.6	346.6	359.9	351.7
Helium temperature, °C	298.6	302.4	318.5	311.9
Cladding temperature at ID, °C	262.5	258.0	277.1	272.0
Mean cladding temperature, °C	205.1	202.5	211.5	208.8
Cladding temperature at OD, °C	154.9	154.2	153.9	153.3

5a, b, f

[redacted]

Table 9 (Cont'd)
Details of 3 Rod Worst Case Target Operations

[redacted]	Peak Power Rod No added Margin	Peak Power Rod Maximum added Margin	Maximum Heating Rod No added Margin	Maximum Heating Rod Maximum added Margin
UO_2 gap conductance, W/(m^2 C)	49643.1	38796.7	49643.1	49643.1
	Peak Power Rod No added Margin	Peak Power Rod Maximum added Margin	Maximum Heating Rod No added Margin	Maximum Heating Rod Maximum added Margin
Coolant HTC, W/(m^2 C)	[redacted]	[redacted]	[redacted]	[redacted]
Water (scallop) OD, mm	14.823	14.823	14.823	14.823
D_h, mm	10.779	9.581	10.779	9.581
Re (D_h)	[redacted]	[redacted]	[redacted]	[redacted]
Local coolant velocity, m/s	[redacted]	[redacted]	[redacted]	[redacted]
Mass flow per rod, kg/s	[redacted]	[redacted]	[redacted]	[redacted]
Mass flow per target, kg/s	[redacted]	[redacted]	[redacted]	[redacted]
Mass flow per target, sgpm	[redacted]	[redacted]	[redacted]	[redacted]
Coolant inlet temperature, °C	41.49	41.49	41.49	41.49
Local coolant temperature, °C	45.32	46.90	46.68	48.81
Coolant outlet temperature, °C	52.31	52.80	56.13	56.79
Local saturation temperature, °C	123.15	122.78	121.00	120.73
Peak pellet power density, W/cc	[redacted]	[redacted]	[redacted]	[redacted]
Heat (modeled) per rod, W	[redacted]	[redacted]	[redacted]	[redacted]
Heat flux at cladding OD, W/m^2	[redacted]	[redacted]	[redacted]	[redacted]
Bernath CHF, W/m^2	[redacted]	[redacted]	[redacted]	[redacted]
Bernath CHFR	2.66	2.65	2.09	2.07
Macbeth CHF, W/m^2	[redacted]	[redacted]	[redacted]	[redacted]
Macbeth CHFR	3.44	3.83	3.05	3.38
Groeneveld CHF, W/m^2	[redacted]	[redacted]	[redacted]	[redacted]
Groeneveld CHFR	2.89	3.00	2.32	2.43
Minimum CHFR	2.665	2.653	2.090	2.067
Pressure at CHFR, atm	2.1645	2.1400	2.0240	2.0063

5a, d, e, f

5a, d, e, f

5a, d, e, f

5a, d, e, f

[redacted]

This same model was also used create a complete rod temperature map to predict the full axial and radial temperature distribution in the rods for the purpose of evaluating the radiation source terms. This was done for nominal conditions without additional calculational margins for 11 rods at 10 MWt and 85% flow for the peak power rod at various axial heights, using the local heat rates (30441R00031) and the local fractions of the heated length and pressure drop. The source term results from this temperature mapping are documented in 30441R00022. The temperatures are shown in Table 10.

[redacted]

Table 10
Full Temperature Map of the UO_2 for the Nominal Peak Power Rod at 10 MWt, 85% Flow

r, mm		0	0.1768	0.3953	0.7374	0.8839	1.1319	1.3807	1.6298	1.879	2.129	2.378	2.5
Node	ht, cm	CL	1	2	3	4	5	6	7	8	9	10	OD
1	1.2	1650.8	1642.9	1617.6	1557.8	1467.3	1348.7	1208.2	1051.9	886.7	718.4	553.1	470.7
2	3.6	1695.1	1686.9	1660.8	1598.9	1504.7	1381.4	1234.7	1071.4	899.0	724.8	554.1	469.3
3	6.0	1863.4	1854.3	1825.2	1755.4	1648.3	1505.5	1333.3	1142.1	942.6	744.1	552.7	458.8
4	8.4	1947.0	1937.5	1907.1	1834.2	1720.5	1568.2	1383.4	1177.1	962.8	751.0	548.6	450.2
5	10.8	1979.5	1969.9	1939.0	1864.9	1748.7	1592.9	1402.8	1190.5	970.1	753.0	546.3	446.1
6	13.2	1995.6	1986.0	1954.8	1880.0	1762.9	1605.2	1412.5	1197.0	973.6	753.8	545.0	443.8
7	15.6	1988.1	1978.5	1947.4	1873.0	1756.3	1599.4	1408.0	1194.0	971.9	753.4	545.6	444.8
8	18.0	2031.4	2021.5	1989.8	1913.7	1794.3	1632.6	1434.0	1211.4	981.0	755.3	541.7	438.6
9	20.4	2021.8	2012.0	1980.5	1904.7	1785.9	1625.3	1428.3	1207.6	979.1	755.0	542.6	440.1
10	22.8	2005.3	1995.6	1964.3	1889.1	1771.3	1612.6	1418.2	1200.8	975.5	754.1	543.9	442.3
11	25.2	1994.0	1984.3	1953.1	1878.4	1761.3	1603.8	1411.4	1196.2	973.0	753.5	544.9	443.8
12	27.6	1928.9	1919.6	1889.4	1817.1	1704.9	1554.4	1372.3	1169.4	958.3	749.4	549.4	451.9
13	30.0	1894.3	1885.1	1855.5	1784.5	1674.9	1528.1	1351.3	1154.7	949.8	746.5	551.1	455.5
14	32.4	1813.9	1805.1	1776.7	1709.3	1605.8	1468.9	1304.1	1120.9	929.6	738.4	553.3	462.1
15	34.8	1798.4	1789.6	1761.5	1694.9	1592.5	1457.5	1295.2	1114.5	925.7	736.8	553.6	463.3
16	37.2	1711.6	1703.3	1676.9	1614.2	1518.5	1393.3	1244.2	1078.1	903.0	726.4	553.7	468.0
17	39.6	1591.9	1584.3	1560.2	1503.4	1417.5	1305.7	1172.8	1025.1	868.6	708.5	549.9	470.6
18	42.0	1457.5	1450.8	1429.4	1379.1	1303.8	1206.2	1090.4	960.8	822.9	680.5	537.1	464.8
19	44.4	1320.3	1314.5	1296.2	1253.1	1188.3	1104.7	1005.3	893.5	773.0	647.8	520.0	454.9
20	46.8	1179.4	1174.6	1159.2	1123.2	1069.3	999.2	915.5	820.8	717.7	609.2	497.7	439.9
21	49.2	1025.0	1021.2	1009.0	980.3	937.2	881.2	813.7	736.5	651.9	561.1	467.0	417.6
22	51.6	887.2	884.2	874.6	852.0	817.9	773.0	719.0	656.7	587.3	512.6	433.8	391.9
23	54.0	775.0	772.6	764.9	746.8	719.3	683.2	639.2	587.9	530.7	468.5	401.8	366.2
24	56.4	666.7	664.8	658.7	644.5	622.8	594.1	559.0	518.2	472.1	421.2	366.1	336.7
25	58.8	642.4	640.6	634.9	621.5	601.0	573.9	540.8	502.1	458.3	409.9	357.6	329.5

A last concern in the design and operation of the target assembly is vibration of the tubes due to the surrounding flow. Conservatively ignoring the stiffening effects of the internal Zircaloy tube filled with the target pellets, the simply supported tubes have a natural frequency of 26 Hz and a

[redacted]

maximum displacement of between 65 μm, using the correlations of Paidoussis (which is also the ASME B&PV Section III, Div 1, Appendix N recommended method), and 4 μm as per the work of Blevins, both of which are reported in Reference 18. These values were provided as input to a structural analysis of the assembly, as reported in 30441R00017.

6 REFERENCES

1 GA Doc. No. 30441R00031 – Moved to Applicable Documents Section

2 GA Doc. No. 3044D000211 – Moved to Applicable Documents Section

3 GA Doc. No. 3044D00207 – Moved to Applicable Documents Section

4 FRAPCON-3.4: A Computer Code for the Calculation of Steady-State, Thermal-Mechanical Behavior of Oxide Fuel Rods for High Burnup (NUREG/CR-7022, Volume 1, PNNL-19418, Volume 1), September 2015

5 "Thermophysical properties Database of materials for light water reactors and heavy water reactors", IAEA, June 2006, p. 89

6 Lemmon, E.W, Huber, M.L., and McLinden, M.O., "REFPROP9 - NIST Reference Fluid Thermodynamic and Transport Properties Database, Version 9", National Institute of Standards and Technology, 2010

7 Dean, R.A., Thermal Contact Conductance Between UO_2 and Zircaloy 2," Carolinas-Virginia Nuclear Power Association Report CVNA-127. Westinghouse Electric Corp., 1962

8 Rader, D.J., et. al., Measurements of Thermal Accommodation Coefficients, Sandia Report SAND2005-6084, October, 2005

9 Cullimore, B.A., Goble, R.G., Jensen, C.I., Ring, S.G., "Sinda85, the Systems Improved Numerical Differencing Analyzer - 1985", Martin Marietta Corporation, 1986

10 GA Doc. No. 30441R00029 – Moved to Applicable Documents Section

11 GA Doc. No. 30441R00038 – Moved to Applicable Documents Section

12 Dirker, J. and Meyer, J.P., Convection in concentric Annular Regions for Turbulent Flow of Liquid Water, R & D Journal, 2003, p. 17-21

13 Jens, W.H., Lottes, P.A., Analysis of Heat Transfer, Burnout, Pressure Drop and Density Data fir High Pressure Water, ANL-4627, May 1, 1951

14 Bernath, L., "A theory of local-boiling burnout and its application to existing data," Chemical Engineering Progress Symposium Series, Vol. 56, No. 30, 1960

15 FRAPTRAN 1.5: "A Computer Code for the Transient Analysis of Oxide Fuel Rods", NUREG/CR-7023, PNNL-19400, Vol. 1. Rev. 1, May 2014

16 Groeneveld, D.C., et al, The 2006 CHF look-up table, Nuclear Engineering and Design 237 (2007) p. 1909-1922

17 GA Doc. No. 30441R00022 – Moved to Applicable Documents Section

18 Farmer, M.T., Hoffman, E.A., Pfeiffer, P.F., Therios, I.U, Wei, T.Y.C., Generation IV Nuclear Energy System Initiative Pin Core Subassembly Design, Argonne National Laboratory, ANL-GenIV-070, April, 2006, p. 57-59

19 GA Doc. No. 30441R00017 – Moved to Applicable Documents Section

Attachment 4

GENERAL ATOMICS
P.O. BOX 85608 SAN DIEGO, CA 92186-5608 (858) 455-3000